

The impact and rotational lightcurves of Comet 9P/Tempel 1

Jean Manfroid¹, Damien Hutsemékers¹, Emmanuël Jehin²,
Anita L. Cochran³, Claude Arpigny¹, William M. Jackson⁴,
Karen J. Meech⁵, Rita Schulz⁶, Jean-Marc Zucconi⁷

1. Institut d'Astrophysique et de Géophysique, Sart-Tilman, B-4000 Liège, Belgium; manfroid@astro.ulg.ac.be; arpigny@astro.ulg.ac.be; hutsemekers@astro.ulg.ac.be
2. European Southern Observatory, Casilla 19001, Santiago, Chile; ejehin@eso.org
3. Department of Astronomy and McDonald Observatory, University of Texas at Austin, C-1400, Austin, USA; anita@barolo.as.utexas.edu
4. Department of Chemistry, University of California, 1 Shields Avenue, Davis, CA 95616; wm-jackson@ucdavis.edu
5. Institute for Astronomy, University of Hawaii at Manoa, 2680 Woodlawn Drive, Honolulu, USA; meech@IfA.Hawaii.Edu
6. ESA/RSSD, ESTEC, P.O. Box 299, NL-2200 AG Noordwijk, The Netherlands; rschulz@rssd.esa.int
7. Observatoire de Besançon, F25010 Besançon Cedex, France; jmz@dalai-zebu.org

Proposed Running Head : The impact and rotational lightcurves of Comet 9P/Tempel 1

First Author address :

Jean Manfroid

Institut d'Astrophysique et de Géophysique

Allée du six août 17, Sart-Tilman

B-4000 Liège, Belgium

manfroid@astro.ulg.ac.be

Abstract

UVES and HIRES high-resolution spectra of comet 9P/Tempel 1 are used to investigate the impact and rotational light curves of various species with a view toward building a simple model of the distribution and activity of the sources. The emission by OH, NH, CN, C₃, CH, C₂, NH₂ and O I, are analyzed, as well as the light scattered by the dust. It is found that a simple model reproduces fairly well the impact lightcurves of all species combining the production of the observed molecules and the expansion of the material throughout the slit. The impact light curves are consistent with velocities of 400–600 m/s. Their modelling requires a three-step dissociation sequence “Grand-Parent → Parent → Daughter” to produce the observed molecules. The rotational light curve for each species is explained in terms of a single model with three sources. The dust component can however not easily be explained that way.

Keywords: Deep Impact – Comets – 9P/Tempel 1

1 Introduction

The Deep Impact (DI) experiment was a first in cometary astrophysics. Instead of observing objects in a relatively steady state, it was possible to watch the instantaneous release of a large quantity of cometary material and its subsequent evolution in timescales of hours and days (A'Hearn et al. 2005). The fact that the time of origin of the observed effects is known, provided an extraordinary advantage in studying the complex evolutive mechanisms governing the physics and chemistry in the coma. The international collaboration also provided the unique opportunity to monitor a comet during weeks with an armada of telescopes (Meech et al. 2005). Here, we present the analysis of data obtained over 15 nights spread before, during and after the Deep Impact event (2005 July 4, 05:52 UT as seen from Earth) with the high-resolution spectrographs of the ESO VLT (European Southern Observatory, Very Large Telescope, Cerro Paranal, Chile) and Keck (Hawaii) observatories. We investigate the impact and the rotational light curves of various emissions and provide a simple model for the activity of the sources. The emission by OH, NH, CN, C₃, CH, C₂, NH₂ and O I, are analyzed, as well as the light scattered by the dust.

The observations are presented in Section 2. The light curves observed immediately after the impact at the Keck I telescope are presented in Section 3 together with their interpretation by a simple model. In Section 4, these light curves are again used to build a model also for the rotational light curves that resulted from the data collected during 13 nights at the VLT. Finally we summarize our conclusions in Section 5.

2 Observations and data reduction

The high-resolution spectra of comet 9P/Tempel 1 obtained with the VLT UVES (ESO UltraViolet Echelle Spectrograph) and Keck I HIRES (High Resolution Echelle Spectrograph) between May and July 2005 are described in Jehin et al (2006), and in Tables 1 and 2. The slits used at both telescopes had similar areas ($10''$ by $0.44''$ for UVES, $7''$ by $0.86''$ for HIRES) and were generally centered on the nucleus, which allows some comparison of the photometric light curves. The reductions were made in the usual manner for cometary spectra. The echelle package of IRAF (Image Reduction and Analysis Facility) and the UVES pipeline (v1.4) implemented in the ESO-MIDAS (Münich Image Data Analysis System) software package (Ballester et al. 2000) were used to extract the various orders. The dust and twilight contributions were subtracted after proper scaling and Doppler shifting of an appropriate solar (UVES) or solar analog (HIRES) spectrum. This was done order by order so that linear wavelength shifts and simple scaling factors could be used. The latter was derived in an iterative procedure until nulling of all remaining solar features.

The spectrographs were not designed to be used as high precision photometers, and the observations were not conducted with the photometric issue as a priority. The centering on the nucleus was not always perfect and the slit width was only a fraction of an arc second. Some UVES spectra were intentionally offset from the nucleus by between 1 and 2 arcsec (see Table 1). This can lead to significant effects on components with a sharp spatial profile (dust). The position of the nucleus along the slit was not quite stable in the HIRES data. A slight drift along the slit occurred during the impact night, partly because of the differential atmospheric refraction (the slit was aligned along the parallactic angle and there was no refraction corrector). At high air mass, in the bluest orders of the last spectra, the nucleus was almost at the edge of the slit.

The main problem was thus to choose the proper extraction aperture. Calculations made with

different apertures showed differences of up to 15 % in the photometric light curve during the impact night. After some testing we found that the most sensible solution was to use the full slit length on both spectrographs, keeping in mind the intrinsic limitations of such measurements. This full aperture could be easily defined from the flat frames and it yielded the maximum signal-to-noise ratio, which is certainly a determining factor for such a faint comet.

From these spectra we derived the flux of major emission bands and of the dust scattered solar spectrum, assuming a clear atmosphere, and stable detectors. Eight gaseous species were measured and analyzed : OH (0-0) at 308 nm, NH (0-0) at 336 nm, CN (0-0) at 388 nm, C₃ complex at 405 and 407 nm, CH (0-0) at 430 nm, C₂ (0-0) band head at 516 nm, various lines of NH₂ at 519, 531, 569, 574 nm, and the green and red oxygen forbidden lines ([O I]) at 558 nm and 630 nm (UVES only). Table 3 details the wavelength ranges of interest where major emission features and the corresponding comparison zones (not always emission free) can be found. The wavelengths are given in the rest frame of the nucleus. For OH, NH and CN the integration was done on a series of individual lines. The [O I] lines have been deblended from the telluric features. Plots of a typical spectrum are shown on Fig. 1.

UVES data were obtained over 13 nights (10 consecutive nights encircling the impact date). This provided complete coverage of the comet's light curve over several rotational periods. As the CN band was covered in all UVES setups, it is the species with the most observations. Other molecules have less dense coverage in the phase diagram. After correcting for the higher efficiency of new mirror coatings and for the strong Swings effect closer to the comet's perihelion, we could directly compare CN fluxes measured in June and July 2005. The comet activity appeared to be slightly higher (about 3 %) in June, for which we corrected the CN data. However, for the other species we used only the July observations, as we could not do reliable adjustments owing

to less available data and/or the lack of accurate models.

The dust contribution has been accurately evaluated in each spectrum in order to perform an accurate continuum subtraction. However, as the small slit width of UVES lead to large variations when the slit was not perfectly centered on the nucleus and/or when the seeing changed, we kept only the well-centered spectra (see Table 1) for evaluation. The HIRES data were obtained with a wider slit and therefore did not show this effect. The main HIRES data set covers the four hours following the impact (see Table 3). In addition three HIRES spectra obtained on May 30 are available ¹.

The relative variations in the brightness of the dust appear to be wavelength independent over the whole spectral range, both in the UVES and HIRES impact data. The data presented here are the same as in Jehin et al (2006).

3 Modelling the impact light curve

The impact light curves were deduced from the HIRES and UVES spectra obtained during the hours (or nights) following the impact. They had to be corrected for the natural rotational variations, which were most important for the spectra obtained during the first hours after the impact as they coincide with the very phase when the natural light curves exhibit the fastest variations of the 1.7 d cycle. The resulting impact light curves are illustrated in Figs. 2–10.

3.1 A simple model

We assume that the observed species –the daughter– originates from a single parent which itself comes from a single grandparent in a continuous sequence of dissociation (the three species coexist at any t). The grandparent appears necessary to introduce a delay in the light curves

¹Those data are publicly available at <http://msc.caltech.edu/deepimpact/>

(cf. Sect. 3.2). Within this framework, we may write

$$\begin{aligned}
 dn_g &= -\alpha_g n_g dt \\
 dn_p &= +\alpha_{gp} n_g dt - \alpha_p n_p dt \\
 dn_d &= +\alpha_{pd} n_p dt - \alpha_d n_d dt
 \end{aligned} \tag{1}$$

from which we derive

$$\frac{n_d}{n_{g_0}} = \frac{\alpha_{pd} \alpha_{gp}}{(\alpha_p - \alpha_d)(\alpha_g - \alpha_d)} e^{-\alpha_d t} + \frac{\alpha_{pd} \alpha_{gp}}{(\alpha_d - \alpha_p)(\alpha_g - \alpha_p)} e^{-\alpha_p t} + \frac{\alpha_{pd} \alpha_{gp}}{(\alpha_d - \alpha_g)(\alpha_p - \alpha_g)} e^{-\alpha_g t}. \tag{2}$$

In these equations, n is the number of molecules, the subscripts d , p , g standing for daughter, parent and grandparent respectively. n_{g_0} is the number of grandparents produced at once by the impact. The grandparent can be anything, e.g. icy grains, complex or simple molecules, as long as it obeys Eq. 1. $\alpha = 1/\tau$ are inverse lifetimes; α_g , α_p and α_d characterize the destruction or dissociation of the grandparent, parent and daughter; α_{gp} and α_{pd} refer to the production of the parent from the dissociation of the grandparent and to the production of the daughter from the dissociation of the parent, accounting for the possibility that the grandparent (resp. parent) may dissociate into several parents (resp. daughters). We then have $\alpha_g = \sum_p \alpha_{gp}$ and $\alpha_p = \sum_d \alpha_{pd}$. If the dissociation lifetime of the daughter is very long compared to the timescale of the event ($\alpha_d \simeq 0$) and if the grandparent does not exist or has a very small lifetime, Eq. 2 will simplify to

$$\frac{n_d}{n_{p_0}} = 1 - e^{-\alpha_p t} \tag{3}$$

which is useful to get a first insight into the observed light curves. In this case, n_{p_0} is the number of parents produced by the impact.

Eqs. 2 and 3 are only valid if all the expanding material is within the slit area. When a part of the material moving at velocity v exits the slit width w , i.e., at $t > t_w = w/2v$, the number

of particles within the slit decreases with time. Assuming that the expanding material forms a shell of radius $v t$, the volume inside and outside the slit area may be readily computed such that for $t > t_w$

$$n'_d = n_d \frac{t_w}{t} \quad (4)$$

where n_d is given by Eq. 2 or 3 (when $t \leq t_w$, $n'_d = n_d$). Although established for a spherical expansion, this relation is also valid for instance for a hemispherical flow. When $t > t_l$, the material fills both the slit width w and the slit length l . Assuming $l \gg w$, we may write

$$n'_d = n_d \frac{t_w}{t} \frac{2}{\pi} \arcsin\left(\frac{t_l}{t}\right) \quad (5)$$

which becomes

$$n'_d = n_d \frac{2}{\pi} \frac{t_w t_l}{t^2} \quad (6)$$

when $t \gg t_l$. In the case of the HIRES data, $t_l = 8.1 t_w$. Assuming the medium to be optically thin, the observed flux is simply proportional to $n'_d(t)$ integrated over the exposure time.

Since it is unlikely that all the material is moving at a single velocity v , we introduce a velocity distribution. For convenience we use

$$dn_{g_0} = N_{g_0} \frac{1}{\sigma_v \sqrt{\pi}} e^{-(v-\bar{v})^2/\sigma_v^2} dv \quad (7)$$

where the mean velocity \bar{v} and its standard deviation σ_v are parameters which can be estimated from the observations. It is important to note that in this simplified model we assume that the daughter, parent and grandparent species expand with the same velocity.

To summarize, we have

$$n'_d(t) = \int N_{g_0} B D(v) R(t) S(v, t) dv \quad (8)$$

integrated over the velocity distribution, with

$$D(v) = \frac{1}{\sigma_v \sqrt{\pi}} e^{-(v-\bar{v})^2/\sigma_v^2}, \quad (9)$$

$$R(t) = \frac{\alpha_p \alpha_g}{(\alpha_p - \alpha_d)(\alpha_g - \alpha_d)} e^{-\alpha_d t} + \frac{\alpha_p \alpha_g}{(\alpha_d - \alpha_p)(\alpha_g - \alpha_p)} e^{-\alpha_p t} + \frac{\alpha_p \alpha_g}{(\alpha_d - \alpha_g)(\alpha_p - \alpha_g)} e^{-\alpha_g t} \quad (10)$$

and

$$\begin{aligned} S(v, t) &= 1 && \text{when } t_w \geq t \\ S(v, t) &= \frac{t_w}{t} && \text{when } t_w < t \text{ and } t_l \geq t \\ S(v, t) &= \frac{t_w}{t} \frac{2}{\pi} \arcsin\left(\frac{t_l}{t}\right) && \text{when } t_l < t \end{aligned} \quad (11)$$

where $t_w = w/2v$, $t_l = l/2v$ and $B = \alpha_{pd}\alpha_{gp}/\alpha_p\alpha_g$. Free parameters are \bar{v} , σ_v , α_d , α_p , α_g and $N_{g_0}B$. Since absolute fluxes are not measured, $N_{g_0}B$ is just a scaling factor. As seen in Eq. 10, $R(t)$ is identical if we exchange the values of α_p and α_g , such that parameter fitting can be done with either $\alpha_g/\alpha_p > 1$ or $\alpha_g/\alpha_p < 1$.

3.2 Interpretation of the light curves

CN – Fig. 2 illustrates the observed post-impact light curve of CN (hereafter the daughter molecule). It is characterized by a rather steep rise and a smooth decline. The maximum corresponds to the time at which the material fills either the slit width or the slit length. At times $t > t_w$ and $t > t_l$, the light curve can be seen as a combination of the production of CN (Eq. 2) and the dilution of the expanding material beyond the slit area (Eqs. 4 or 5). At large t we may neglect, to first approximation, the effect of the grandparent as well as the CN dissociation lifetime, which is very long (Fray et al. 2005 and references therein) — probably longer than 4 days (Keller et al. 2005). Therefore Eq. 3 holds at large t . In this case, the number of daughter molecules may be constant after some time (as long as $\alpha_p t \ll 1$ in Eq. 3) or proportional to t (if $\alpha_p t \gg 1$). We then expect the shape of the decline of the light curve to be roughly intermediate between a constant and t^{-1} if the bump corresponds to the filling of

the slit width (Eqs. 3 & 4) or between t^{-1} and t^{-2} if the bump corresponds to the filling of the slit length (Eqs. 3 & 6). However, since the velocity of the flow is not unique the situation is less cut-clear and an independent knowledge of the bulk velocity of the flow is needed.

In the case of CN, the analysis of the spatial profiles has led us (Jehin et al. 2006) to estimate the velocity of the expanding material to $\bar{v} \simeq 400$ m/s (with a range of projected velocities from 250 to 650 m/s). Since the $0.86'' \times 7.0''$ HIRES slit corresponds to $562 \text{ km} \times 4570 \text{ km}$ at the comet at the epoch of the observations, the slit length is filled after $t_l = 0.066$ d, which corresponds to the bump seen in the light curve. The fact that the decline of the light curve is not as steep as t^{-2} indicates that the CN production still continues at $t > t_l$ which requires a rather long lifetime for its parent. If the material is expanding at a single velocity ($\sigma_v \ll \bar{v}$), we will expect a sharp decline just after filling the slit, i.e., a relatively narrow bump. The fact that such a bump is not observed requires some smoothing, i.e. a large velocity dispersion. After some trial we find that $\sigma_v \gtrsim 100$ m/s is needed to reproduce the data, which is in agreement with initial estimates (Jehin et al. 2006).

As illustrated in Fig. 2, modelling the CN light curve with only a parent molecule results in a much faster rise after the impact and a clear discontinuity at $t \simeq t_w$, when the material leaves the slit width. Such models cannot reproduce the data whatever values are adopted for the lifetimes. A grandparent must be added to introduce a delay in the light curve just after the impact. In Fig. 2a, we show reasonable fits to the data with different combinations of α_p and α_g/α_p , indicating some degeneracy between α_p and α_g . The value of the parent lifetime needed to reproduce the data, does not only depend on the ratio α_g/α_p , but also on the adopted velocity distribution. Fig. 2a shows an equally acceptable fit with $\sigma_v = 200$ m/s. In general, adding material at lower velocities enhances the number of molecules in the slit at $t > t_l$, and consequently requires a shorter parent lifetime to fit the data.

Although we are able to reproduce fairly well the observed light curve, the parent lifetime $\tau_p = 1/\alpha_p$ that we derive appears very uncertain owing to the strong dependence on both the velocity distribution and the ratio α_g/α_p . Without additional data and/or independent constraints, the CN parent dissociation lifetimes, which we estimate from acceptable fits, are roughly in the range 0.1 – 10 d. Fortunately, additional measurements from UVES observations were performed several hours after the impact allowing us to constrain further the model (Fig. 2b). We find that models with $0.2 \text{ d}^{-1} \lesssim \alpha_p \lesssim 4 \text{ d}^{-1}$ are favoured, which corresponds to CN parent dissociation lifetimes of $2 \cdot 10^4 \text{ s} \lesssim \tau_p \lesssim 5 \cdot 10^5 \text{ s}$. Even with this additional constraint, the derived lifetimes are accurate only within orders of magnitude. They are consistent with other estimates (Keller et al. 2005, Fray et al. 2005) and with the hypothesis that HCN is the parent of CN. The CN grandparent destruction lifetime is even more uncertain, providing no information on its nature.

Figures 3–9 illustrate the light curves of the other molecules and [OI]. The modelling is essentially similar to the one discussed in detail for CN. When necessary, the velocity distribution is fine tuned in order to reach the best fit. Indeed, differences can arise in, e.g., the dissociation process. Additional details are briefly described below while the derived parameters are gathered in Table 4.

OH – In Fig. 3 the photometry obtained with the Optical Monitor (OM) of the XMM-Newton satellite (Schulz et al. 2006) has been included. The simultaneous fit of HIRES and XMM-OM data requires a velocity of the OH radicals comparable to the velocity of CN. We then adopt 400 m/s for the material to exit the HIRES slit length at $t_l = 0.066 \text{ d}$ and the XMM-OM aperture at $t_w = 0.056 \text{ d}$. Models of the light curve are not very sensitive to the long OH dissociation

lifetime ($\tau_d \sim 2 \cdot 10^5$ s at $r_h = 1.5$ AU, from Morgenthaler et al. 2001) and require both a grandparent and a parent (Fig. 3). Acceptable models reproduce fairly well the data with the parent and grandparent destruction lifetimes given in Table 4, which, as in the case of CN, appear to be poorly determined. The OH parent dissociation lifetimes we derive largely encompass the dissociation lifetime of H₂O ($\sim 8 \cdot 10^4$ s), a possible parent of OH.

NH₂ – The relatively narrow bump in the NH₂ light curve (Fig. 4) suggests a slightly higher velocity with a not too high dispersion. We adopt $\bar{v} = 500$ m/s and $\sigma_v = 100$ m/s. A range of acceptable combinations of α_p and α_g is given in Table 4. The long NH₂ dissociation lifetime has little effect on the models ($\tau_d > 1.5 \cdot 10^5$ s at $r_h = 1.5$ AU, from Cochran et al. 1992). The derived NH₂ parent lifetimes are poorly determined and are consistent with other estimates (e.g. Wyckoff et al. 1988, Fink et al. 1991).

NH – A slightly higher velocity is needed to reproduce the data; we adopt $\bar{v} = 550$ m/s and $\sigma_v = 150$ m/s (Fig. 5). The long NH dissociation lifetime has little effect on the models ($\tau_d > 1 \cdot 10^5$ s from Schleicher et al. 1989). The derived NH parent dissociation lifetimes are consistent with other estimates (e.g. Schleicher et al. 1989).

C₃ – Keeping in mind the large uncertainties of the flux measurements (cf. the measurements just after the impact), acceptable models can reproduce the data with $\bar{v} \simeq 400$ m/s (Fig. 6). A range of acceptable combinations of α_p and α_g is given in Table 4. The long C₃ dissociation lifetime has little affect on the models ($\tau_d > 3 \cdot 10^5$ s at $r_h = 1.5$ AU from Cochran et al. 1992). The rather short C₃ parent dissociation lifetimes we derive are consistent with other estimates (e.g., Rauer et al. 2003, Randall et al. 1992).

C₂ – A higher velocity is needed to reproduce the data; we adopt $\bar{v} = 650$ m/s and $\sigma_v = 200$ m/s (Fig. 7). However the measurements are very uncertain and should be seen with caution. The long C₂ dissociation lifetime has little effect on the models ($\tau_d > 3 \cdot 10^5$ s at $r_h = 1.5$ AU from Cochran et al. 1992). The derived C₂ parent dissociation lifetimes are consistent with other estimates (Combi and Fink 1997 and references therein).

CH – While the range of the adopted CH parent and grandparent lifetimes (Table 4) reproduces reasonably well the major part of the light curve (given the uncertainties) and agrees with other estimates (e.g. Cochran et al. 1992), the relatively short CH dissociation lifetime used in the modelling ($\tau_d > 1 \cdot 10^4$ s at $r_h = 1.5$ AU, from Cochran et al. 1992) might be underestimated since the residual flux at $t \simeq 0.85$ d cannot be fitted by the model (Fig. 8b). However the measurements for CH are very uncertain and should be regarded with caution.

OI – Photodissociation of molecules like H₂O, OH, CO₂ or CO can produce OI directly in the excited ¹D and ¹S states (Festou and Feldman 1981, Morgenthaler et al. 2001). These metastable states have a lifetime of ~ 110 s and ~ 0.74 s, respectively, much shorter than the photodissociation lifetime of the parent molecules. Those atoms travel only a short distance before decaying to the ground state and emitting photons at 6300Å (and 6364 Å) and at 5577Å respectively.

In the modelling procedure, we first considered OI atoms as the daughter species. However, given the very short lifetime of the metastable levels, the light curve actually traces the parent molecule, such that one stage in the 3-step dissociation sequence used up to now is lost. Such models provide poor fits essentially because the computed light curves are rising too fast just

after the impact. When considering either OH or CO as the “daughter” species –with rather long dissociation lifetimes– and H₂O or CO₂ as the “parents”, coming themselves from unknown grandparents released by the impact, acceptable fits of the light curve are obtained (Fig. 9) with various combinations of α_p and α_g (Table 4). While the information the derived lifetimes provide on the parent species is only limited, the fact that a 3-step dissociation sequence is needed to reproduce the data suggests that OI (¹S) atoms are not produced directly from the dissociation of H₂O or CO₂, but through OH or CO. Moreover, the OI light curve is not similar to the one of OH (Fig. 3). This might indicate a significant contribution from the CO₂ → CO dissociation sequence.

3.3 The dust light curve

The variations of the dust after the impact are much faster than for the gas, with a very steep brightening (Fig. 10). The maximum is already reached at about UT 06:18 ± 10 min, the dust being at that time enhanced by a factor of ~ 8.5 with respect to the pre-impact spectrum. The decline of the dust emission may also be interpreted as the escape of dust from the slit. This would give a projected dust velocity of ~ 0.18 ± 0.05 km/s, as, in this case, the escape from the slit width is the dominant factor. However the slow and quasi linear decline would require a rather broad range of velocities – slower than the gas component – and/or complex processes like destruction of highly reflective icy grains by sunlight. Similar dust outflow projected velocities were deduced from the analysis of the radial profiles (~ 0.13 ± 0.03 km/s, Jehin et al. 2006) and from the evolution of the dust cloud (~ 0.18 – 0.2 km/s, Meech et al. 2005 and references therein; ~ 0.13 – 0.23 km/s Schleicher et al. 2006), .

4 Modelling the rotational light curve

A preliminary analysis of the CN light curve from the UVES data (Fig. 11) revealed a periodicity of 1.709 ± 0.009 d and the presence of three main sources or active regions (Jehin et al. 2006). We constructed phase diagrams with the above period using the time origin of the impact as seen from Earth, July 4, UT 05:52. In order to allow comparisons, all data were normalized to unity at impact time, i.e., at phase 0. The spectrum obtained at impact is strongly affected by twilight and yields noisier data. Hence, the May data were included in the phase diagram to fix the zero point.

We want to test the hypothesis that the light curve $f_s(t)$ of the comet in the wavelength of different species (s) can be represented as the response of the comet to a continuous succession of infinitesimal impact-like events. This is merely a way of describing the instantaneous production rates of the active regions under the influence of the solar radiation modulated by the rotation of the nucleus. We assume a linear behavior, i.e., $f_s(t)$ is the linear superposition of the transitory responses to the series of micro-events:

$$f_s(t) = \int_{-\infty}^t g_s(t') n_s(t-t') dt' \quad (12)$$

where $n_s(t)$ is the impact light curve (Eq. 8) corresponding to species s and $g_s(t)$ represents the total instantaneous activity of all sources. $g_s(t) = g_s(t+P)$ and $f_s(t) = f_s(t+P)$ are periodic functions of period P . We assume that there is a finite number N of sources. Their contribution can be described as

$$g_s(t') = \sum_{i=1}^N b_{s,i}(t' - t_{s,i}) + g_{s,0} \quad (13)$$

where the $b_{s,i}(t) = b_{s,i}(t+P)$ are the rates of activity of the N sources, and $g_{s,0}$ is a possible

background of activity.

The decomposition into discrete sources arises from physical considerations, i.e., the idea that the cometary material comes from several areas or vents. It also allows us to use simple functions $b(t)$ since one might expect the activity of each source to exhibit periodic rise and fall cycles. One may also expect the various sources to have similar behavior, so the same function could be used with some phase shift.

It must be emphasized that, because impact and rotational light curves overlap for several days, they must be disentangled through an iterative process, which adds some complexity to the modelling procedure.

The following conclusions were reached using the simplest satisfactory model, i.e., the one with fewest free parameters.

- The two main maxima of the light curves suggest the presence of at least two sources. In fact, three sources are necessary to explain the general shape of the light curves, i.e., $N = 3$. Using only two sources leads to a pronounced gap in the light curve.

- There is no residual activity $g_{s,0} = 0$
- The activity of each source follows the same pattern during the rotation of the nucleus, i.e., we can write :

$$b_{s,i}(t) = a_{s,i}b_s(t) \tag{14}$$

with the $b_s(t)$ independent of i .

- This activity of each source can be approximated by an intermittent function, a variant of

a triangular wave. With $0 \leq \tau_{s,1} \leq \tau_{s,2} \leq P$, we write in the interval $0 \leq t \leq P$:

$$b_s(t) = \begin{cases} = t/\tau_{s,1} & \text{if } 0 < t \leq \tau_{s,1} \\ = (\tau_{s,2} - t)/(\tau_{s,2} - \tau_{s,1}) & \text{if } \tau_{s,1} < t \leq \tau_{s,2} \\ = 0 & \text{if } \tau_{s,2} < t \leq P \end{cases} \quad (15)$$

This function repeats itself at each interval $kP \leq t \leq (k+1)P$.

- The onset times of each source are the same for each species, $t_{s,i} = t_i = (0.18P, 0.47P, 0.85P) + kP$
- The relative intensity of each source is the same for all species, i.e., $a_{s,i} = c_s d_i$ with $d_i = (0.4, 0.7, 1.0)$. This is equivalent with the relative production rates of each species being the same for each source, i.e., the material is the same.
- The long-term characteristic time-scale of the decay of $n_s(t)$ is strongly correlated with the overall amplitude of the light curve s . This provides an independent way of predicting the residuals in the post-impact nights.
- Finally, $\tau_{s,1}$ and $\tau_{s,2}$, describing the activity of the sources, are very similar for all species. We found that the best fits are obtained with two sets of parameters. For CN, CH and [O I] we find $\tau_{s,1} = 0.21P$ and $\tau_{s,2} = 0.39P$ while for OH, NH, NH₂, C₂, C₃, $\tau_{s,1} = 0.19P$ and $\tau_{s,2} = 0.35P$. The rise and fall are quasi symmetrical.

The above conclusions apply to the gas only. The dust cannot be described by the same model. The phase diagram shows almost no hint of periodicity whereas a fit with the above parameters and the response $n_{\text{dust}}(t)$ observed after the impact would give very strong variations (see Fig. 11, bottom). This means that either (i) the temporal variation of the dust luminosity observed after the impact, $n_{\text{dust}}(t)$, is not representative of the response of the dust ejected

from the sources, or (ii) the modulation is masked by a very large residual component ($g_{\text{dust},0}$) of non-volatile dust.

5 Discussion and conclusions

The high-resolution spectra obtained with the UVES and HIRES spectrographs have provided photometric data of unexpectedly good quality, in view of the faintness of the target, the limited area of the slits and the less than perfect centering. This allowed us to model the impact as well as the rotational light curve of this comet which led to the following conclusions.

- Within the uncertainties a simple model reproduces fairly well the impact light curves of all species. The light curve may reflect the combination of the production of the observed species and the expansion of the material throughout the slit.
- All impact light curves are consistent with $\bar{v} \simeq 400\text{--}600$ m/s ($\sigma_v = 100\text{--}200$ m/s). NH and NH₂ have similar light curves and slightly higher velocities, possibly indicating a common origin.
- With these expansion velocities, a three-step dissociation sequence “Grand-Parent \rightarrow Parent \rightarrow Daughter” is necessary and sufficient to model all light curves.
- The exact nature of the grandparents is unknown. It can be anything which desintegrates (or sublimates) as e^{-t/τ_g} . The order of magnitude of its destruction lifetime is typically 10⁴s. It could be common to all species (e.g., icy dust grains released by the impact).
- Parent lifetimes can only be determined to better than an order of magnitude. They largely encompass the various parent lifetimes proposed in the literature.

- The gas activity is generated by three sources, whose duration is less than about 0.4 of the period, i.e., compatible with a daylight excitation.
- The activity of each source follows a similar pattern.
- The progressive increase and decrease of the activity of each source is compatible with the modulation of the incidence angle of the solar radiation.
- The dust observed during the impact disappears rapidly and is probably mostly sublimating water ice in fragments with a diverse size distribution.
- The dust observed after the impact is dominated by another, less volatile component, which may consist of the core of slow-moving dust particles that have lost their icy component and are weakly bound to the nucleus.
- The material releasing CN, CH and OI seems to be present during a slightly longer period than that responsible of OH, NH, NH₂, C₂, C₃.

6 Acknowledgments

Based on observations carried out at the European Southern Observatory (ESO) under prog. 075.C-0355(A), this program was part of a joint European initiative in support of the NASA DEEP IMPACT mission to comet 9P/Tempel 1 by ground-based observations at La Silla and VLT Paranal. Some of the material presented here is based on data obtained at the W. M. Keck Observatory, which immediately made its data available to the public after impact occurred on July 4, 2005. The W. M. Keck Observatory is operated as a scientific partnership among the California Institute of Technology, the University of California and the National Aeronautics and Space Administration. The Observatory was made possible by the generous financial support of

the W.M. Keck Foundation. The authors wish to recognize and acknowledge the very significant cultural role and reverence that the summit of Mauna Kea has always had within the indigenous Hawaiian community. We are most fortunate to have the opportunity to get observations from this mountain. JM is Research Director and DH is Research Associate at FNRS (Belgium).

References

- [1] A'Hearn, M. F. and 32 additional authors 2005. Deep Impact : Excavating Comet Tempel 1. *Science* **310**, 258-264.
- [2] Ballester, P., Modigliani, A., Boitquin, O., Cristiani, S., Hanuschik, R., Kaufer, A., and S. Wolf 2000. The UVES Data Reduction Pipeline. *The Messenger* **101**, 31-36.
- [3] Cochran, A. L., Barker, E. S., Ramseyer, T. F., and A. D. Storrs 1992. The McDonald Observatory Faint Comet Survey - Gas production in 17 comets. *Icarus* **98**, 151-162.
- [4] Combi, M. R., and U. Fink 1997. A Critical Study of Molecular Photodissociation and CHON Grain Sources for Cometary C₂. *ApJ* **484**, 879-890.
- [5] Festou M.C., Feldman P.D. 1981, The Forbidden Oxygen Lines in Comets *AA* **103**, 154-159
- [6] Fink, U., Combi, M. R., and M. A. DiSanti 1991. Comet P/Halley - Spatial distributions and scale lengths for C₂, CN, NH₂, and H₂O. *ApJ* **383**, 356-371.
- [7] Fray, N., Bénilan, Y., Cottin, H., Gazeau, M.-C., Crovisier 2005, The origin of the CN radical in comets : A review from observations and models. *Planetary and Space Science* **53**, 1243-1262

- [8] Jehin, E., Manfroid, J., Hutsemékers, D., Cochran, A. L., Arpigny, C., Jackson, W. M., Rauer, H., Schulz, R., and J.-M. Zucconi 2006. Deep Impact : High Resolution Optical Spectroscopy with the ESO VLT and the Keck I Telescope. *ApJ* **641**, 145-148.
- [9] Keller H. U. and 11 additional authors 2005. Deep Impact Observations by OSIRIS Onboard the Rosetta Spacecraft. *Science* **310**, 281-283.
- [10] Meech, K. J. and 208 additional authors 2005. Deep Impact : Observations from a worldwide earth-based campaign. *Science* **310**, 265-269.
- [11] Morgenthaler, J. P., Harris, W. M., Scherb, F., Anderson, C. M., Oliverson, R. J., Doane, N. E., Combi, M. R., Marconi, M. L., and W. H Smyth 2001. Large-Aperture [O I] 6300 Å Photometry of Comet Hale-Bopp: Implications for the Photochemistry of OH. *ApJ* **563**, 451-461.
- [12] Randall, C. E., Schleicher, D. G., Ballou, R. G., and D. J. Osip 1992. Observational Constraints on Molecular Scalelengths and Lifetimes in Comets. *BAAS* **24**, 1002.
- [13] Schleicher, D. G., Barnes, K. L., Baugh, N. F. 2006. Photometry and Imaging Results for Comet 9P/Tempel 1 and Deep Impact: Gas Production Rates, Postimpact Light Curves, and Ejecta Plume Morphology. *Astronomical Journal* 131, 1130-1137.
- [14] Rauer, H. and 12 additional authors 2003. Long-term optical spectrophotometric monitoring of comet C/1995 O1 (Hale-Bopp). *A&A* **397**, 1109-1122.
- [15] Schulz, R., Owens, A., Rodriguez-Pascual, P. M., Lumb, D., Erd, C., and J. A. Stüwe 2006. Detection of water ice grains after the DEEP IMPACT onto Comet 9P/Tempel 1. *A&A* **448**, 53-56.

- [16] Schleicher, D. G., and R. L. Millis, R.L. 1989. Revised scale lengths for cometary NH. *ApJ* **339**, 1107-1114.
- [17] Wyckoff, S., Tegler, S., Wehinger, P. A., Spinrad, H., and M.J.S. Belton 1988. Abundances in Comet Halley at the time of the spacecraft encounters. *ApJ* **325**, 927-38.

Table 1: UVES data observational circumstances

UT Date (start) 2005-mm-dd	Setup (nm)	Exp. (s)	Airm.	Slit PA (deg.)	Off. (")	r (AU)	Δ (AU)	\dot{r} (km/s)	$\dot{\Delta}$ (km/s)	PsAng (deg.)
06-02 / 00:23:14	346+580	5400	1.14	117.7	0.0	1.54	0.76	-3.7	5.3	117.4
06-02 / 01:59:22	437+860	5400	1.17	117.7	0.0	1.54	0.76	-3.6	5.5	117.4
06-07 / 00:36:14	346+580	5400	1.11	116.3	0.0	1.53	0.78	-3.2	6.0	116.3
06-07 / 02:10:49	437+860	5400	1.20	0.0	0.0	1.53	0.78	-3.2	6.1	116.3
06-08 / 00:47:19	346+580	5400	1.11	116.0	0.0	1.53	0.78	-3.1	6.2	116.0
06-08 / 02:27:26	437+860	5400	1.25	0.0	0.0	1.53	0.78	-3.1	6.3	116.0
07-02 / 22:54:56	350+580	7200	1.05	21.5	1.1	1.51	0.89	-0.3	8.9	115.5
07-03 / 00:58:58	437+860	7200	1.11	21.5	1.2	1.51	0.89	-0.3	9.2	115.5
07-03 / 22:54:01	350+580	7200	1.05	21.5	1.0	1.51	0.89	-0.2	9.0	111.4
07-04 / 00:58:31	437+860	7200	1.11	21.5	1.4	1.51	0.89	-0.1	9.0	111.4
07-04 / 22:54:47	348+580	7200	1.05	21.5	0.9	1.51	0.90	0.0	9.2	111.3
07-05 / 01:01:27	437+860	7800	1.12	111.5	1.9	1.51	0.90	0.0	9.4	111.3
07-06 / 00:10:42	348+580	9600	1.05	135.0	1.3	1.51	0.90	0.1	9.5	111.1
07-06 / 02:54:53	437+860	4800	1.60	135.0	0.0	1.51	0.90	0.1	9.7	111.1
07-06 / 22:55:07	348+580	7500	1.04	111.0	0.0	1.51	0.91	0.2	9.4	111.0
07-07 / 01:03:45	437+860	7500	1.13	111.0	0.0	1.51	0.91	0.2	9.6	111.0
07-07 / 22:50:59	348+580	7500	1.04	21.0	0.0	1.51	0.91	0.3	9.6	110.9
07-08 / 00:59:17	437+860	7500	1.12	21.0	0.0	1.51	0.91	0.3	9.8	110.9
07-08 / 22:54:05	348+580	7500	1.03	21.0	0.0	1.51	0.92	0.4	9.7	110.7
07-09 / 01:03:09	437+860	7500	1.13	21.0	0.0	1.51	0.92	0.4	9.9	110.7
07-09 / 22:51:16	348+580	7800	1.03	21.0	0.0	1.51	0.92	0.5	9.8	110.6
07-10 / 01:05:21	437+860	7800	1.14	21.0	0.0	1.51	0.93	0.6	10.0	110.6
07-10 / 22:52:20	348+580	7200	1.03	21.0	0.0	1.51	0.93	0.7	9.9	110.5
07-11 / 00:59:27	437+860	7200	1.12	21.0	0.0	1.51	0.93	0.7	10.2	110.5
07-11 / 22:54:57	348+580	7200	1.03	21.0	0.0	1.51	0.94	0.8	10.0	110.3
07-12 / 00:58:51	437+860	7200	1.13	21.0	0.0	1.51	0.94	0.8	10.3	110.3

r is the heliocentric distance in astronomical units (AU) and Δ is the geocentric distance, \dot{r} is the heliocentric radial velocity, Exp. is the the total exposure time in seconds, Airm. is the air-mass at mid exposure, Slit PA is the slit position angle (North to East), Off. is the offset of the slit center from the nucleus, PsAng is the position angle of the Sun-Comet vector. The Setup column defines the central wavelength of the UVES blue and red arm.

Table 2: HIRES data observational circumstances

UT Date (start) 2005-mm-dd	Exp. (s)	Airm.	Slit PA (deg.)	r (AU)	Δ (AU)	\dot{r} (km/s)	$\dot{\Delta}$ (km/s)	PsAng (deg.)
05-30 / 08:33:06	1200	1.19	59.3	1.55	0.75	-4.0	5.1	118.6
05-30 / 08:54:02	1200	1.26	63.3	1.55	0.75	-4.0	5.1	118.6
05-30 / 09:14:55	1200	1.35	66.3	1.55	0.75	-4.0	5.2	118.6
07-04 / 05:36:15	720	1.16	11.6	1.51	0.89	-0.1	9.1	111.4
07-04 / 05:55:18	600	1.18	20.1	1.51	0.89	-0.1	9.1	111.4
07-04 / 06:06:12	600	1.19	24.8	1.51	0.89	-0.1	9.2	111.4
07-04 / 06:17:05	900	1.22	29.7	1.51	0.89	-0.1	9.2	111.4
07-04 / 06:32:59	900	1.25	35.5	1.51	0.89	-0.1	9.2	111.4
07-04 / 06:48:52	900	1.29	40.6	1.51	0.89	-0.1	9.2	111.4
07-04 / 07:04:46	900	1.35	45.0	1.51	0.89	-0.1	9.3	111.4
07-04 / 07:20:41	900	1.41	48.9	1.51	0.89	-0.1	9.3	111.4
07-04 / 07:36:35	900	1.49	52.3	1.51	0.89	-0.1	9.3	111.4
07-04 / 07:52:29	900	1.59	55.2	1.51	0.89	-0.1	9.3	111.4
07-04 / 08:08:25	900	1.71	57.8	1.51	0.89	-0.1	9.4	111.4
07-04 / 08:24:19	900	1.87	60.0	1.51	0.89	-0.1	9.4	111.4
07-04 / 08:40:13	1800	2.19	65.3	1.51	0.89	-0.1	9.4	111.4
07-04 / 09:11:09	1800	2.88	68.6	1.51	0.89	-0.1	9.4	111.3

Table 3: The gaseous species analyzed

Species	Central windows		Side windows		Extinction Paranal / Mauna Kea (mag/airm)
	(Å)		Blue side	Red side	
OH	3093.4-	96.8	3092.0- 93.2	3097.0- 98.0	1.60 / 1.37
NH	3353.2-	54.4	3352.2- 53.2	3354.2- 55.0	0.62 / 0.54
	3357.2-	58.8	3355.5- 57.2	3358.8- 60.0	0.62 / 0.54
	3364.6-	65.5	3363.4- 64.5	3365.3- 66.3	0.62 / 0.54
	3368.8-	69.5	3367.5- 68.5	3369.5- 70.4	0.62 / 0.54
CN	3876.1-	82.0	3874.9- 75.7	3882.7- 83.7	0.35 / 0.29
C ₃	4048.9-	55.0	4047.4- 48.9	4054.4- 56.9	0.27 / 0.24
	4051.3-	52.2	4047.9- 49.4	4053.4- 54.9	0.27 / 0.24
	4071.9-	75.9	4070.9- 71.9	4075.9- 76.9	0.27 / 0.24
CH	4299.9-	00.6	4298.9- 99.9	4299.6- 01.2	0.22 / 0.19
	4303.9-	04.1	4301.9- 02.9	4304.4- 05.4	0.22 / 0.19
C ₂	5164.5-	65.4	5163.2- 64.4	5165.4- 66.8	0.14 / 0.13
NH ₂	5185.9-	86.4	5184.8- 85.8	5186.8- 87.8	0.14 / 0.13
	5193.8-	94.3	5192.8- 93.8	5194.3- 95.3	0.14 / 0.13
	5731.4-	32.1	5729.8- 30.6	5732.3- 33.3	0.12 / 0.12
[OI]	5577.0-	77.5	5576.0- 77.0	5578.0- 79.0	0.13 / 0.12
	6299.5-	01.0	6299.0- 99.5	6301.0- 02.0	0.07 / -

Table 4: Results of model fitting

	\bar{v} (m/s)	σ_v (m/s)	τ_p (s)	τ_p/τ_g
CN	400	100–200	2–50 10^4	1.1–100
OH	400	200	2–40 10^4	1.1–100
NH ₂	500	100	6–30 10^3	0.01–0.9
C ₃	400	200	8–30 10^3	0.01–0.9
CH	400	200	1–20 10^4	1.1–100
NH	550	150	3–100 10^4	1.1–100
C ₂	650	200	4–200 10^4	1.1–100
OI	400	100	6–90 10^3	1.1–50

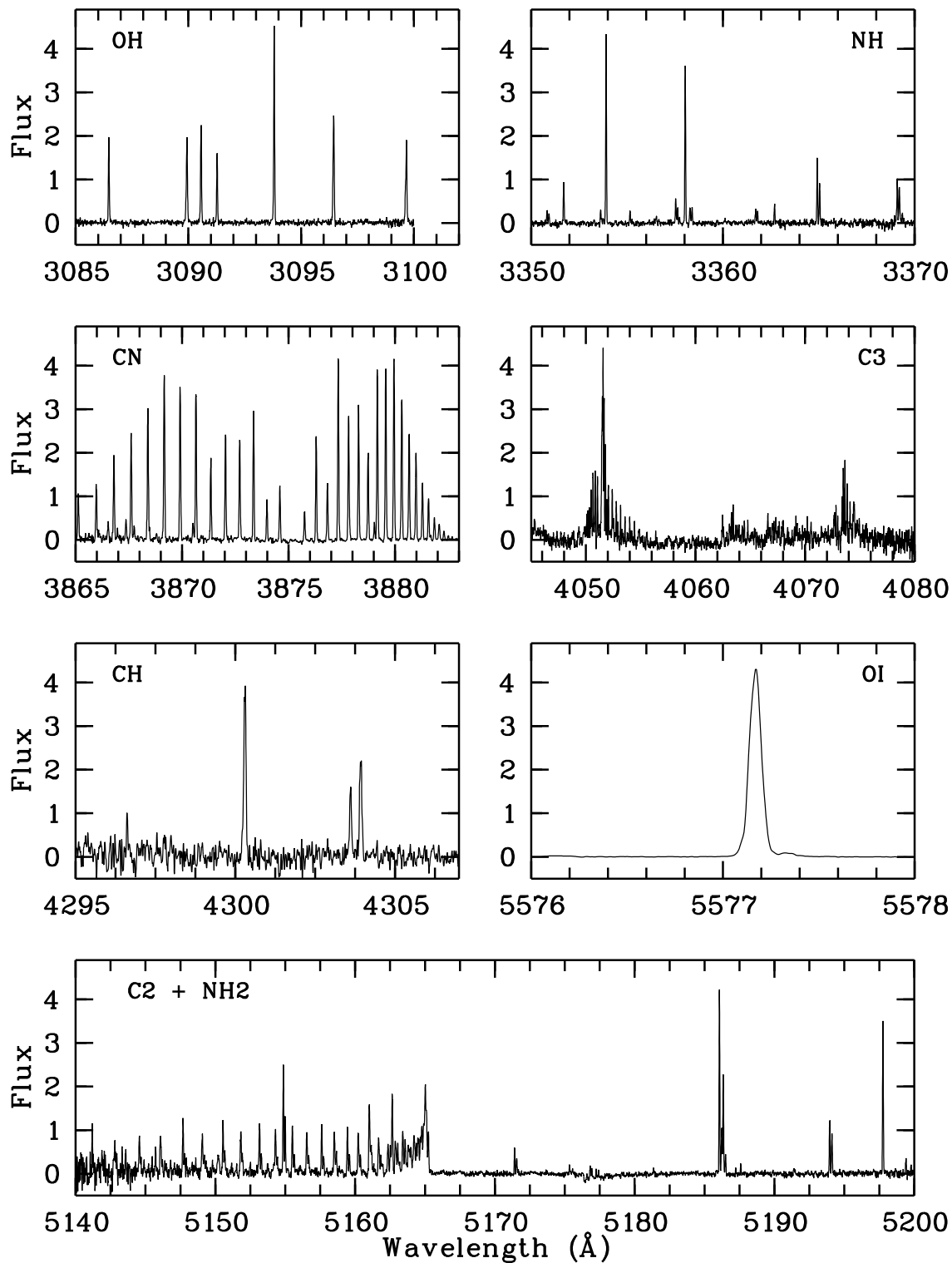


Figure 1: Spectral features used to measure the various species. They are extracted from spectra taken with UVES the night following the impact. The flux is given in arbitrary units.

The cometary [OI] is the small bump on the red wing of the strong telluric line. Most of the

band blueward of 517 nm is C2, while most of the lines above 518 nm are NH₂ ([NI] 519.8 nm

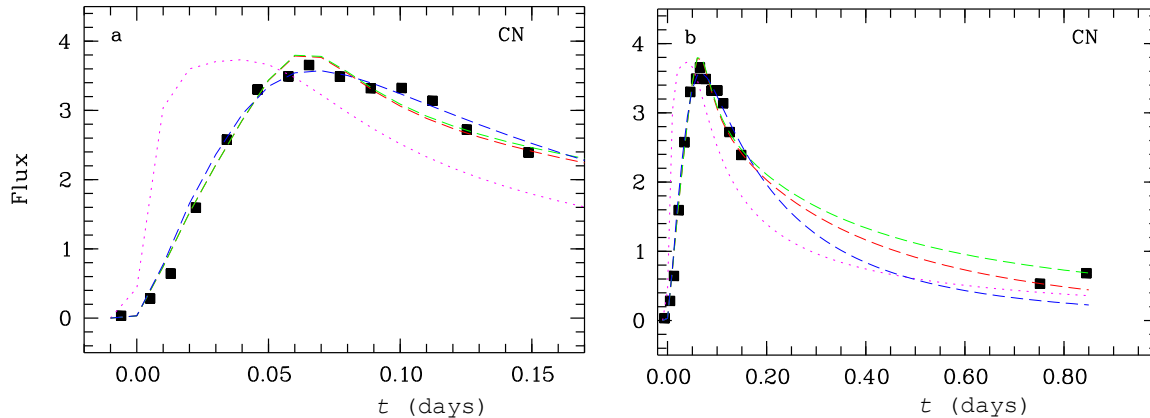


Figure 2: The observed CN light curve in arbitrary units. In this figure and in the following ones, t is the time elapsed since the impact. The superimposed dashed lines are examples of model fitting. In all cases $\bar{v} = 400$ m/s and $\alpha_d = 0.2$ d $^{-1}$. Model 1 (red) is computed with $\sigma_v = 100$ m/s, $\alpha_p = 2$ d $^{-1}$ and $\alpha_g/\alpha_p = 4$. Model 2 (green) is computed with $\sigma_v = 100$ m/s, $\alpha_p = 0.1$ d $^{-1}$ and $\alpha_g/\alpha_p = 100$. Model 3 (blue) is computed with $\sigma_v = 200$ m/s, $\alpha_p = 5$ d $^{-1}$ and $\alpha_g/\alpha_p = 4$. Model 4 (dotted pink) has no grandparent ($\sigma_v = 200$ m/s, $\alpha_p = 0.1$ d $^{-1}$) and is clearly unable to reproduce the data. Fig. 2b shows the better agreement of model 1 with the two later UVES measurements (scaled to the HIRES slit area).

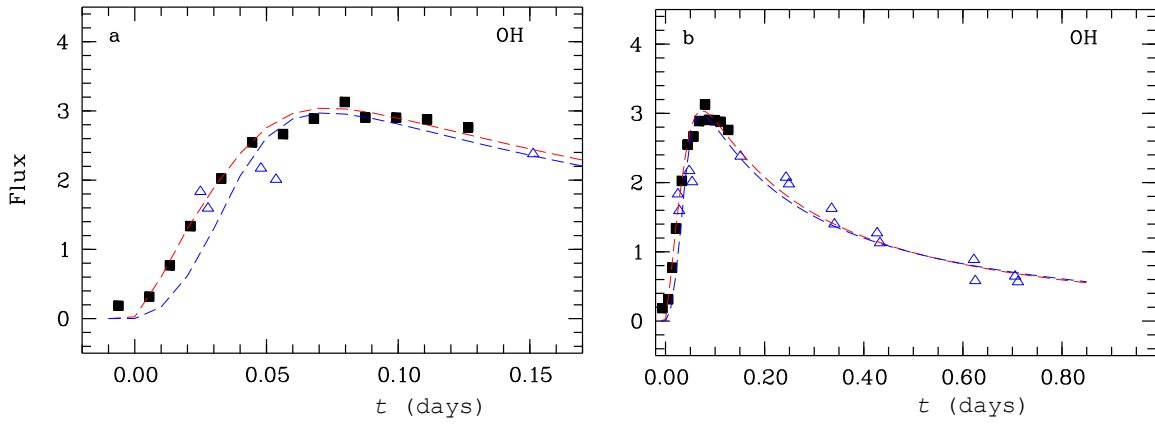


Figure 3: The observed OH light curve in arbitrary units. The triangles are scaled data from Schulz et al. (2006). Model 1 (red) is computed with $\bar{v} = 400$ m/s, $\sigma_v = 200$ m/s, $\alpha_d = 0.4$ d $^{-1}$, $\alpha_p = 0.5$ d $^{-1}$ and $\alpha_g/\alpha_p = 40$. Model OM1 (blue) uses the same parameters but it is adapted to the circular aperture of 6'' (3900 km) used by Schulz et al. (2006) and scaled to correspond to model 1 at large t (with a circular aperture, Eq. 5 must be replaced by $n'_d = n_d (1 - \sqrt{1 - (t_w/t)^2})$).

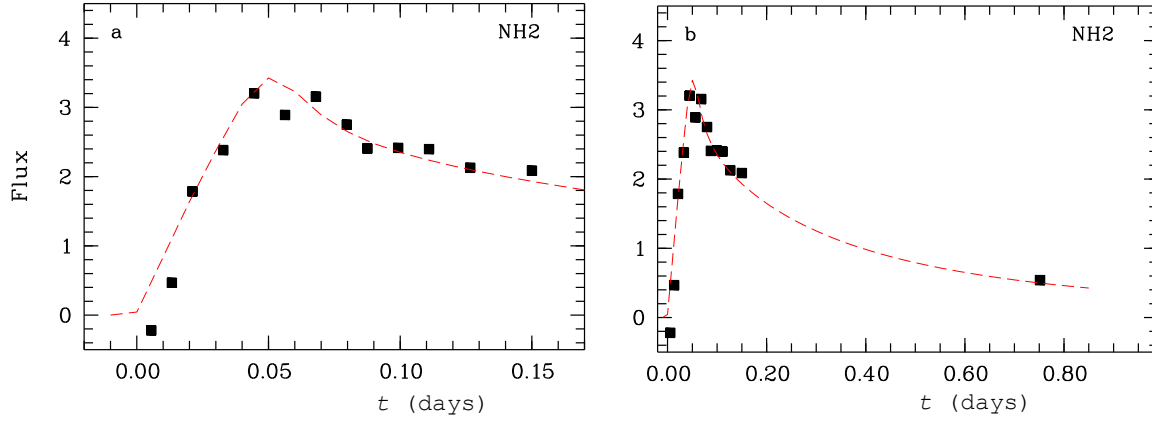


Figure 4: The observed NH_2 light curve in arbitrary units. The illustrated model is computed with $\bar{v} = 500$ m/s, $\sigma_v = 100$ m/s, $\alpha_d = 0.6$ d $^{-1}$, $\alpha_p = 10$ d $^{-1}$ and $\alpha_g/\alpha_p = 0.05$.

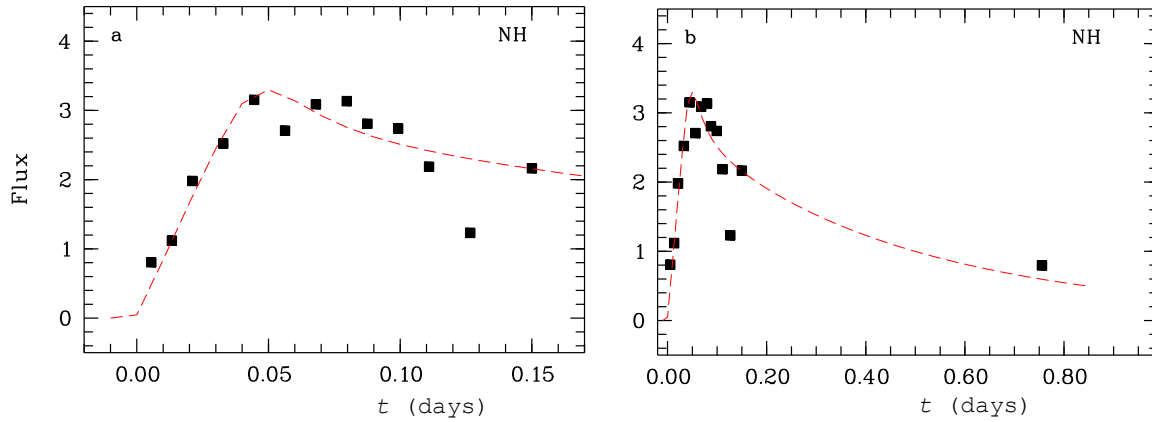


Figure 5: The observed NH light curve in arbitrary units. The illustrated model is computed with $\bar{v} = 550$ m/s, $\sigma_v = 150$ m/s, $\alpha_d = 0.8$ d $^{-1}$, $\alpha_p = 2$ d $^{-1}$ and $\alpha_g/\alpha_p = 2$.

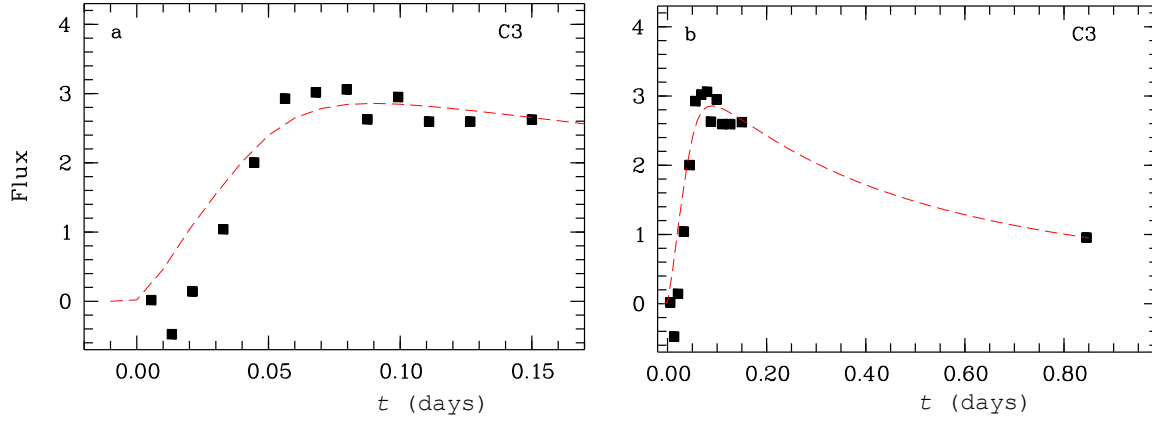


Figure 6: The observed C_3 light curve in arbitrary units. The illustrated model is computed with $\bar{v} = 400$ m/s, $\sigma_v = 200$ m/s, $\alpha_d = 0.3$ d $^{-1}$, $\alpha_p = 10$ d $^{-1}$ and $\alpha_g/\alpha_p = 0.01$.

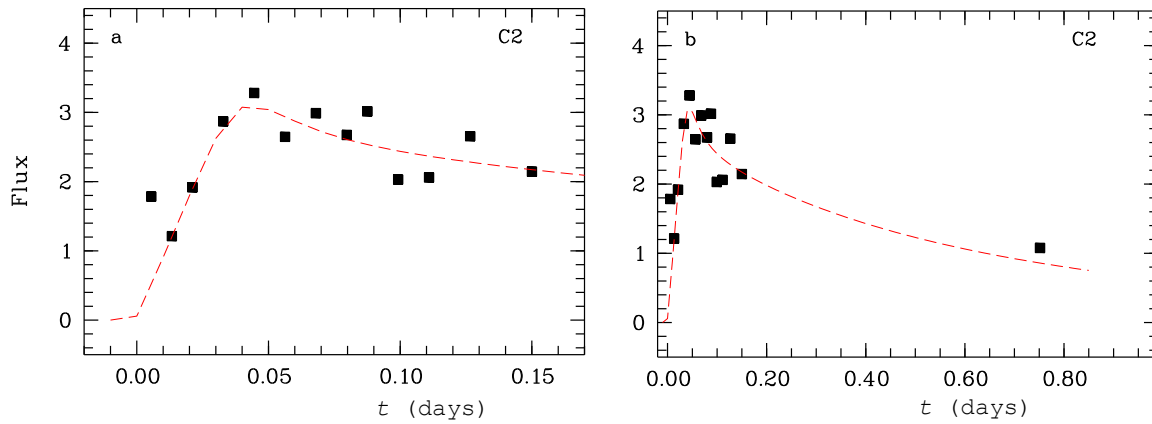


Figure 7: The observed C_2 light curve in arbitrary units. The illustrated model is computed with $\bar{v} = 650$ m/s, $\sigma_v = 200$ m/s, $\alpha_d = 0.3$ d $^{-1}$, $\alpha_p = 1$ d $^{-1}$ and $\alpha_g/\alpha_p = 4$.

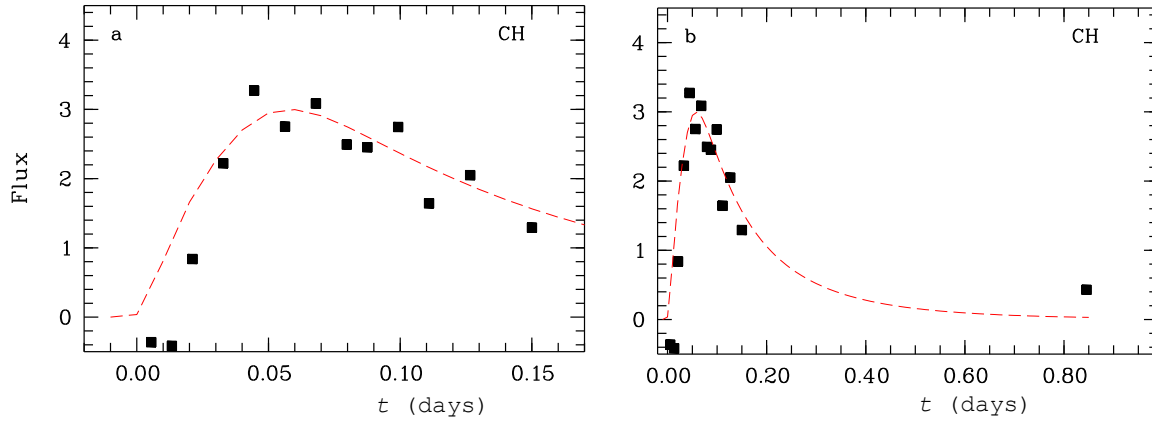


Figure 8: The observed CH light curve in arbitrary units. The illustrated model is computed with $\bar{v} = 400$ m/s, $\sigma_v = 200$ m/s, $\alpha_d = 8.0$ d⁻¹, $\alpha_p = 2$ d⁻¹ and $\alpha_g/\alpha_p = 15$.

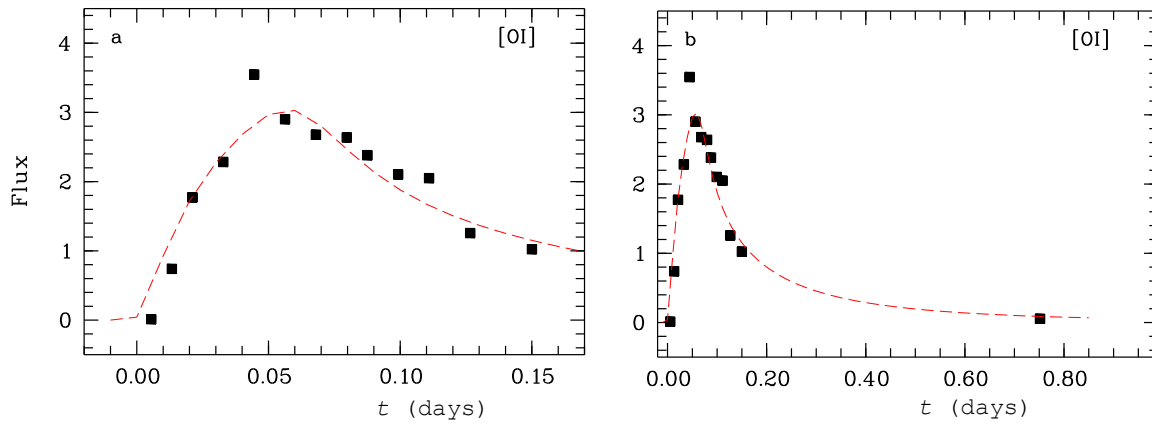


Figure 9: The observed [OI] 5577 Å light curve in arbitrary units. The illustrated model is computed with $\bar{v} = 400$ m/s, $\sigma_v = 100$ m/s, $\alpha_d = 0.4$ d⁻¹, $\alpha_p = 4$ d⁻¹ and $\alpha_g/\alpha_p = 10$.

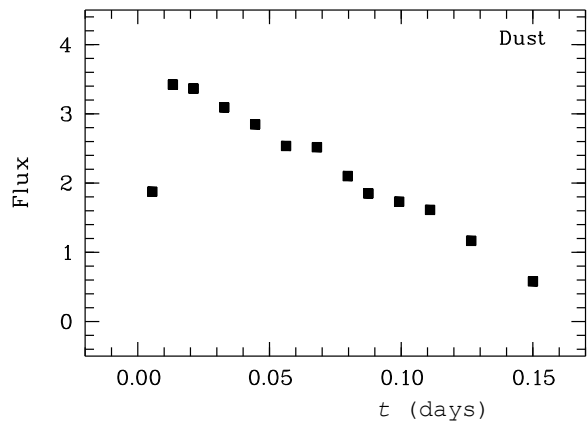


Figure 10: The observed dust light curve in arbitrary units.

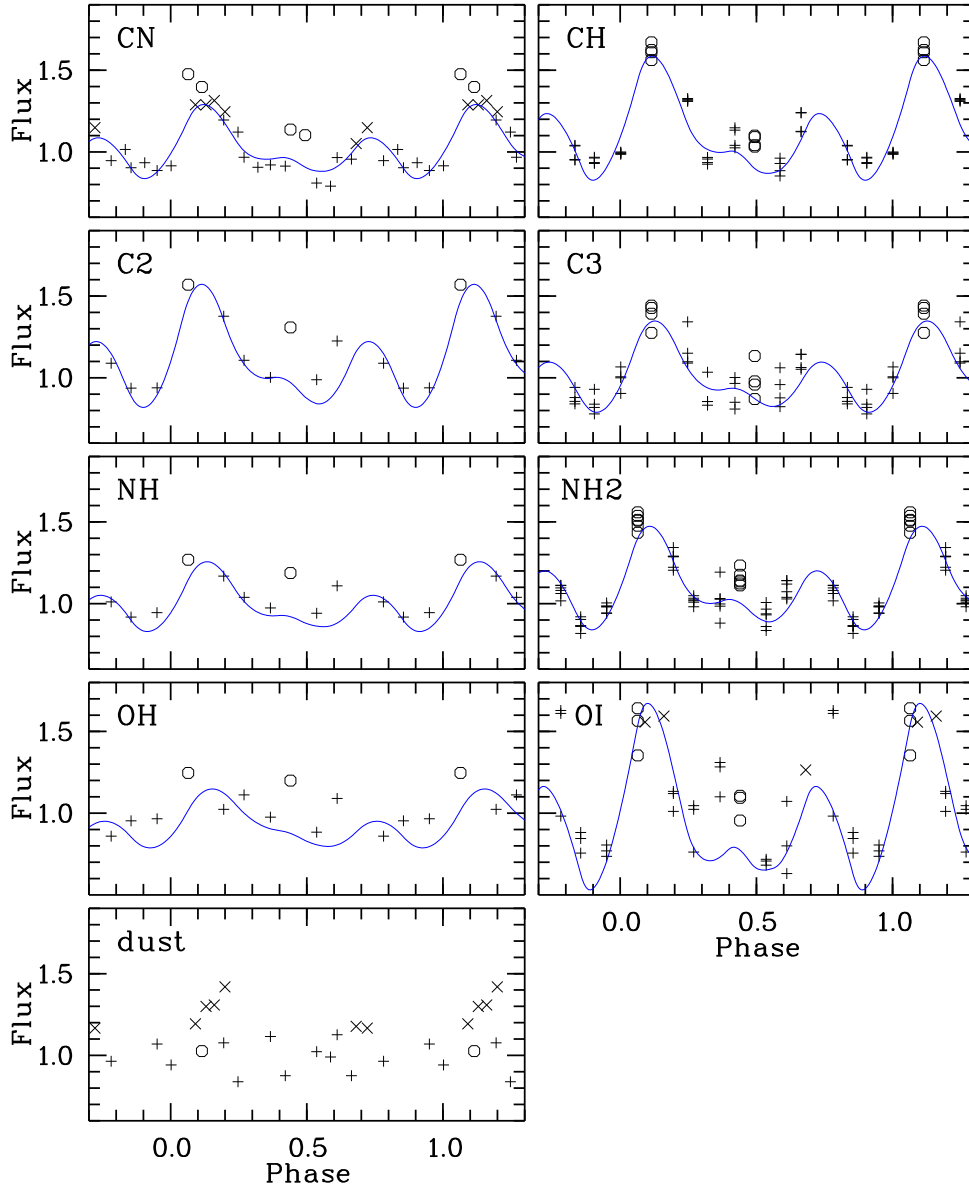


Figure 11: Phase diagrams of the various species. The phase origin coincides with the impact, and the period is 1.709 d. The measurements obtained during the first post-impact nights (first night at phase ~ 0.45 , second night at ~ 0.05) are denoted by circles. The curve is a fit with a three-source model optimized for the whole data set, not for a particular molecule (see text). Hence some fits may look rather poor, because the S/N of the data is bad (e.g., OH). The dust does not show periodic variations, but the June data appear to be systematically higher. The latter are denoted by a different symbol (\times). The flux has been scaled to reach ~ 1 at phase origin.